

# Kaniadakis holographic dark energy: observational constraints and global dynamics

A. Hernández-Almada<sup>1</sup> \*, Genly Leon<sup>2</sup>, Juan Magaña<sup>3</sup>, Miguel A. García-Aspeitia<sup>4,5,6</sup>,  
V. Motta<sup>7</sup>, Emmanuel N. Saridakis<sup>8,9,10</sup>, Kuralay Yesmakhanova<sup>10,11</sup>

<sup>1</sup>Facultad de Ingeniería, Universidad Autónoma de Querétaro, Centro Universitario Cerro de las Campanas, 76010, Santiago de Querétaro, México,

<sup>2</sup>Departamento de Matemáticas, Universidad Católica del Norte, Avda. Angamos 0610, Casilla 1280 Antofagasta, Chile,

<sup>3</sup>Instituto de Astrofísica & Centro de Astro-Ingeniería, Pontificia Universidad Católica de Chile, Av. Vicuña Mackenna, 4860, Santiago, Chile,

<sup>4</sup>Depto. de Física y Matemáticas, Universidad Iberoamericana Ciudad de México, Prolongación Paseo de la Reforma 880, México D. F. 01219, México

<sup>5</sup>Universidad Autónoma de Zacatecas, Calzada Solidaridad esquina con Paseo a la Bufa S/N C.P. 98060, Zacatecas, México,

<sup>6</sup>Consejo Nacional de Ciencia y Tecnología, Av. Insurgentes Sur 1582. Colonia Crédito Constructor, Del. Benito Juárez C.P. 03940, Ciudad de México, México,

<sup>7</sup>Instituto de Física y Astronomía, Facultad de Ciencias, Universidad de Valparaíso, Avda. Gran Bretaña 1111, Valparaíso, Chile,

<sup>8</sup>National Observatory of Athens, Lofos Nymfon, 11852 Athens, Greece,

<sup>9</sup>CAS Key Laboratory for Researches in Galaxies and Cosmology, Department of Astronomy, University of Science and Technology of China, Hefei, Anhui 230026, P.R. China,

<sup>10</sup>Ratbay Myrzakulov Eurasian International Centre for Theoretical Physics, Nur-Sultan 010009, Kazakhstan,

<sup>11</sup>Eurasian National University, Nur-Sultan Astana 010008, Kazakhstan.

Last updated 2020 June 10; in original form 2013 September 5

## ABSTRACT

We investigate Kaniadakis-holographic dark energy by confronting it with observations. We perform a Markov Chain Monte Carlo analysis using cosmic chronometers, supernovae type Ia, and Baryon Acoustic Oscillations data. Concerning the Kaniadakis parameter, we find that it is constrained around zero, namely around the value in which Kaniadakis entropy recovers standard Bekenstein-Hawking one. Additionally, for the present matter density parameter  $\Omega_m^{(0)}$ , we obtain a value slightly smaller compared to  $\Lambda$ CDM scenario. Furthermore, we reconstruct the evolution of the Hubble, deceleration and jerk parameters extracting the deceleration-acceleration transition redshift as  $z_T = 0.86^{+0.21}_{-0.14}$ . Finally, performing a detailed local and global dynamical system analysis, we find that the past attractor of the Universe is the matter-dominated solution, while the late-time stable solution is the dark-energy-dominated one.

**Key words:** Holographic Dark Energy, Observational Constraints, Dynamical System Analysis, Kaniadakis entropy

## 1 INTRODUCTION

The acceleration of the Universe is one of the most elusive problems in modern cosmology. Since its discovery in the last decade of the twentieth century by Supernovae (SNIa) observations (Riess et al. 1998; Perlmutter et al. 1999), and its confirmation by the acoustic peaks of the cosmic microwave background (CMB) radiation (Spergel et al. 2003), it has been a theoretical and observational challenge to construct a model that combines all of its characteristics. From a theoretical point of view, and assuming homogeneous and isotropic symmetries (cosmological principle), the need for a component with features able to reproduce the Universe acceleration is vital to obtain accurate values for the observable Universe age and size. Recently, the confidence in the detection of this acceleration at late times has been increased with precise observations of the large scale structure (Nadathur et al. 2020).

The best candidate to explain the observed acceleration is the well-known Cosmological Constant (CC), interpreted under the assumption that quantum vacuum fluctuations generate the constant energy

density observed and, with this, a late-time acceleration. However, when we apply the Quantum Field Theory to assess the energy density, the result is in total discrepancy with observations, giving rise to the so-called *fine-tuning problem* (Zel'dovich et al. 1968; Weinberg 1989). In addition, recent observations developed by the collaboration *Supernova  $H_0$  for the Equation of State* (SH0ES) (Riess et al. 2021) show a discrepancy for the obtained value of  $H_0$  when compared to Planck observations based on the  $\Lambda$  Cold Dark Matter ( $\Lambda$ CDM) model (Aghanim et al. 2018). This generates a tension of  $4.2\sigma$  between the mentioned experiments, bringing a new crisis and the need for new ways to tackle the problem (Di Valentino et al. 2021), as long as this discrepancy is not related to unknown systematic errors affecting the measurements (Shajib et al. 2020; Birrer & Treu 2021; Efstathiou 2021; Freedman 2021; Shah et al. 2021). Is in this vein that the community has been proposing other alternatives to address the problem of the Universe acceleration. In general, there are two main directions that one could follow. The first is to maintain general relativity and introduce new peculiar forms of matter, such as scalar fields (Copeland et al. 2006; Cai et al. 2010; Motta et al. 2021), Chaplygin gas (Chaplygin 1904; Villanueva 2015; Hernández-Almada, A. et al. 2019), viscous fluids (Cruz et al.

\* Contact e-mail: [ahalmada@uaq.mx](mailto:ahalmada@uaq.mx)

2017a,b, 2019; Hernández-Almada 2019; Hernández-Almada et al. 2020b,a), etc, collectively known as dark-energy sector. The second way is to construct modified gravitational theories (Saridakis et al. 2021; Capozziello & De Laurentis 2011) such as braneworlds models (Maartens & Koyama 2010; García-Aspeitia et al. 2017; García-Aspeitia et al. 2018), emergent gravity (Li & Shafieloo 2019; Pan et al. 2019; Li & Shafieloo 2020; Hernández-Almada et al. 2020c; García-Aspeitia et al. 2019; García-Aspeitia et al. 2021), Einstein-Gauss-Bonnet (Glavan & Lin 2020; García-Aspeitia & Hernández-Almada 2021), thermodynamical models (Saridakis & Basilakos 2021; Leon et al. 2021), torsional gravity (Cai et al. 2016),  $f(R)$  theories (Dainotti et al. 2021), etc.

On the other hand, there is an increasing interest in dark energy alternative models with the holographic principle. This is inspired by the relation between entropy and the area of a black hole. It states that the observable degree of freedom of a physical system in a volume can be encoded in a lower-dimensional description on its boundary ('t Hooft 1993; Susskind 1995). The holographic principle imposes a connection between the infrared (IR) cutoff, related to large-scale of the Universe, with the ultraviolet (UV) one, related to the vacuum energy. Application of the holographic principle to the Universe horizon gives rise to a vacuum energy of holographic origin, namely holographic dark energy (Li 2004; Wang et al. 2017). Holographic dark energy proves to lead to interesting phenomenology and, thus, it has been studied in detailed (Li 2004; Wang et al. 2017; Horvat 2004; Pavon & Zimdahl 2005; Wang et al. 2005; Nojiri & Odintsov 2006; Kim et al. 2006; Setare & Saridakis 2009, 2008), confronted to observations (Zhang & Wu 2005; Li et al. 2009; Feng et al. 2007; Zhang 2009; Lu et al. 2010; Micheletti 2010) and extended to various frameworks (Gong 2004; Saridakis 2008b; Cai 2007; Setare & Vagenas 2008; Saridakis 2008a; Suwa & Nihei 2010; Bouhmadi-Lopez et al. 2011; Khurshudyan et al. 2014; Saridakis 2018; Nojiri & Odintsov 2017; Saridakis et al. 2018; Kritpetch et al. 2020; Saridakis 2020; Dabrowski & Salzano 2020; da Silva & Silva 2021; Mamon et al. 2021; Bhattacharjee 2021; Huang et al. 2021; Lin 2021; Colgáin & Sheikh-Jabbari 2021; Nojiri et al. 2021; Shekh 2021).

Recently, an extension of the holographic dark energy scenario was constructed in (Drepanou et al. 2021), based on Kaniadakis entropy. The latter is an extended entropy arising from the relativistic extension of standard statistical theory, quantified by one new parameter (Kaniadakis 2002, 2005). In the case where this Kaniadakis parameter becomes zero, i.e. when Kaniadakis entropy becomes the standard Bekenstein-Hawking entropy, Kaniadakis-holographic dark energy recovers standard-holographic dark energy, however, in the general case, it exhibits a range of behaviors with interesting cosmological implications.

In this work, we investigate Kaniadakis-holographic dark energy, in order to tackle the late time universe acceleration problem. The outline of the paper is as follows. In Section 2 the mathematical background of the model is considered, presenting the master equations. Section 3 presents the observational confrontation analysis that includes three data samples and the results from the corresponding constraints. Section 4 is dedicated to the dynamical system investigation and the stability analysis. Finally, in Section 5 we give a brief summary and a discussion of the results. Throughout the manuscript we use natural units where  $\tilde{c} = \hbar = k_B = 1$  (unless stated otherwise).

## 2 KANIADAKIS HOLOGRAPHIC DARK ENERGY

In this section we briefly review Kaniadakis holographic dark energy and we elaborate the corresponding equations in order to bring

them to a form suitable for observational confrontation. The essence of holographic dark energy is the inequality  $\rho_{DE} L^4 \leq S$ , with  $\rho_{DE}$  being the holographic dark energy density,  $L$  the largest distance (typically a horizon), and  $S$  the entropy expression in the case of a black hole with a horizon  $L$  (Li 2004; Wang et al. 2017). In the standard application using Bekenstein-Hawking entropy  $S_{BH} \propto A/(4G) = \pi L^2/G$ , where  $A$  is the area and  $G$  the Newton's constant, one obtains standard-holographic dark energy, i.e.  $\rho_{DE} = 3c^2 M_P^2 L^{-2}$ , where  $M_P^2 = (8\pi G)^{-1}$  is the Planck mass and  $c$  is the model parameter arising from the saturation of the above inequality.

On the other hand, one can construct the one-parameter generalization of the classical entropy, namely Kaniadakis entropy  $S_K = -k_B \sum_i n_i \ln_{\{K\}} n_i$  (Kaniadakis 2002, 2005), where  $k_B$  is the Boltzmann constant and with  $\ln_{\{K\}} x = (x^K - x^{-K})/2K$ . This is characterized by the dimensionless parameter  $-1 < K < 1$ , which accounts for the relativistic deviations from standard statistical mechanics, and in the limit  $K \rightarrow 0$  it recovers standard entropy. Kaniadakis entropy can be re-expressed as (Abreu et al. 2016, 2018; Abreu & Ananias Neto 2021)

$$S_K = -k_B \sum_{i=1}^W \frac{P_i^{1+K} - P_i^{1-K}}{2K}, \quad (1)$$

where  $P_i$  is the probability of a specific microstate of the system and  $W$  the total number of possible configurations. Applied in the black-hole framework, it results into (Drepanou et al. 2021; Moradpour et al. 2020; Lympetris et al. 2021)

$$S_K = \frac{1}{K} \sinh(KS_{BH}), \quad (2)$$

which gives standard Bekenstein-Hawking entropy in the limit  $K \rightarrow 0$ . Finally, since any deviations from standard thermodynamics are expected to be small, one can approximate (2) for  $K \ll 1$ , acquiring (Drepanou et al. 2021)

$$S_K = S_{BH} + \frac{K^2}{6} S_{BH}^3 + O(K^4). \quad (3)$$

In order to analyze the dynamics of the universe, we consider the homogeneous and isotropic cosmology based on the Friedmann-Lemaître-Robertson-Walker (FLRW) line element  $ds^2 = -dt^2 + a(t)(dr^2 + r^2 d\Omega^2)$ , where  $d\Omega^2 \equiv d\theta^2 + \sin^2 \theta d\varphi^2$ ,  $a(t)$  is the scale factor and we consider null spatial curvature  $k = 0$ . Furthermore, as usual we use  $L$  as the future event horizon  $R_h \equiv a \int_t^\infty \frac{1}{a(s)} ds$ . Inserting these into the above formulation, and using Kaniadakis entropy instead of Bekenstein-Hawking one, we extract the energy density of Kaniadakis holographic dark energy as (Drepanou et al. 2021)

$$\rho_{DE} = \frac{3c^2 M_P^2}{R_h^2} + K^2 M_P^6 R_h^2, \quad (4)$$

with  $c > 0$  and  $K$  being the two parameters of the model. Hence, we can write the Friedmann and Raychaudhuri equations as

$$H^2 = \frac{1}{3M_P^2} (\rho_m + \rho_{DE}), \quad (5)$$

$$\dot{H} = -\frac{1}{2M_P^2} (\rho_m + p_m + \rho_{DE} + p_{DE}), \quad (6)$$

where  $H \equiv \dot{a}/a$  is the Hubble parameter,  $\rho_m$  and  $p_m$  are the energy density and pressure of matter perfect fluid, while the matter conservation leads to dark energy conservation and, in turn, to the dark

energy pressure

$$p_{DE} = -\frac{2c^2 M_p^2}{R_h^3 H} - \frac{c^2 M_p^2}{R_h^2} + K^2 M_p^6 \left[ \frac{2R_h}{3H} - \frac{5}{3} R_h^2 \right]. \quad (7)$$

The combination of Raychaudhuri equation (6) and (4), (7) gives

$$\begin{aligned} \dot{H} &= \frac{c^2}{R_h^3 H} + \frac{c^2(3w_m + 1)}{2R_h^2} - \frac{3}{2}(w_m + 1)H^2 \\ &\quad - K^2 M_p^4 \left[ \frac{R_h}{3H} - \frac{1}{6} R_h^2(3w_m + 5) \right], \end{aligned} \quad (8)$$

where  $w_m \equiv p_m/\rho_m$  is the equation of state (EoS) parameter for matter, considered from now on as dust ( $w_m = 0$ ). From this expression we can construct the deceleration and jerk parameters, which give us information about the transition to an accelerated Universe. Thus, using the definition of  $R_h$ , we obtain that the energy density is

$$\rho_{DE} = \frac{3c^2 M_p^2}{a^2 \left( \int_t^\infty \frac{1}{a(s)} ds \right)^2} + K^2 M_p^6 a^2 \left( \int_t^\infty \frac{1}{a(s)} ds \right)^2, \quad (9)$$

and the pressure

$$\begin{aligned} p_{DE} &= -\frac{2c^2 M_p^2}{a^3 H \left( \int_t^\infty \frac{1}{a(s)} ds \right)^3} - \frac{c^2 M_p^2}{a^2 \left( \int_t^\infty \frac{1}{a(s)} ds \right)^2} \\ &\quad + K^2 M_p^6 \left[ \frac{2a \left( \int_t^\infty \frac{1}{a(s)} ds \right)}{3H} - \frac{5}{3} a^2 \left( \int_t^\infty \frac{1}{a(s)} ds \right)^2 \right]. \end{aligned} \quad (10)$$

Moreover, the fractional energy density of DE is defined as

$$\Omega_{DE} := \frac{\rho_{DE}}{3M_p^2 H^2} = \frac{K^2 M_p^6 a^4 \left( \int_t^\infty \frac{1}{a(s)} ds \right)^4 + 3c^2 M_p^2}{3M_p^2 a^2 H^2 \left( \int_t^\infty \frac{1}{a(s)} ds \right)^2}. \quad (11)$$

From definition (11) we have four branches for

$$\mathcal{I}(t) := \int_t^\infty a(s)^{-1} ds, \quad (12)$$

which give four possible expressions for the particle horizon

$$R_{h1,2}(t) = \mp \frac{\left[ 3H^2 \Omega_{DE} - \sqrt{9H^4 \Omega_{DE}^2 - 12c^2 K^2 M_p^4} \right]^{1/2}}{\sqrt{2}|K|M_p^2}, \quad (13)$$

$$R_{h3,4}(t) = \mp \frac{\left[ 3H^2 \Omega_{DE} + \sqrt{9H^4 \Omega_{DE}^2 - 12c^2 K^2 M_p^4} \right]^{1/2}}{\sqrt{2}|K|M_p^2}. \quad (14)$$

$R_{h1}(t)$  and  $R_{h3}(t)$  are both discarded since they lead to negative particle horizon. To decide between the choices  $R_{h2}(t)$  and  $R_{h4}(t)$ , which are both non negative, we calculate the limit  $K \rightarrow 0$  and obtain

$$\lim_{K \rightarrow 0} R_{h2} = \frac{c}{H\sqrt{\Omega_{DE}}}, \quad \lim_{K \rightarrow 0} R_{h4} = \infty. \quad (15)$$

That is,  $R_{h2}(t)$  defined by (13) is the only physical solution.

We proceed by introducing the usual dimensionless variable

$$E \equiv \frac{H}{H_0}, \quad (16)$$

where  $H_0$  is the Hubble constant at present time and, for convenience,

$$\text{we define the dimensionless constant } \beta \equiv \frac{KM_p^2}{H_0^2}.$$

Differentiating (11) and (16), and using the Friedmann equations we obtain the master equations

$$\Omega'_{DE} = (1 - \Omega_{DE}) [3(w_m + 1)\Omega_{DE} + 2\mathcal{X}], \quad (17)$$

$$E' = E \left[ -\frac{3}{2}(w_m + 1)(1 - \Omega_{DE}) + \mathcal{X} \right], \quad (18)$$

where

$$\begin{aligned} \mathcal{X} &\equiv \frac{1}{E^3} \left[ \frac{2\beta^2 E^4 \Omega_{DE}^2 - 8\beta^4 c^2/3}{3E^2 \Omega_{DE} - \sqrt{9E^4 \Omega_{DE}^2 - 12\beta^2 c^2}} \right]^{1/2} \\ &\quad - \frac{1}{E^2} [E^4 \Omega_{DE}^2 - 4\beta^2 c^2/3]^{1/2}. \end{aligned} \quad (19)$$

We use initial conditions  $\Omega_{DE}(0) \equiv \Omega_{DE}^{(0)} = 1 - \Omega_m^{(0)}$ ,  $E(0) = 1$ , where primes denote derivatives with respect to e-foldings number  $N = \ln(a/a_0)$ , and  $N = 0$  marks the current time (from now on, the index ‘‘0’’ marks the value of a quantity at present). The physical region of the phase space is

$$3E^4 \Omega_{DE}^2 - 4\beta^2 c^2 \geq 0. \quad (20)$$

Notice that  $\mathcal{X} \rightarrow \frac{\Omega_{DE}^{3/2}}{c} - \Omega_{DE}$  as  $\beta \rightarrow 0$ .

From the matter conservation equation, we arrive at

$$\rho'_m(N) = -3(1 + w_m)\rho_m, \quad \rho_m(0) = 3M_p^2 H_0^2 \Omega_m^{(0)}, \quad (21)$$

and, therefore, we have  $\rho_m(N) = 3H_0^2 M_p^2 \Omega_m^{(0)} e^{-3N(w_m+1)}$  which then leads to

$$\Omega_{DE}(N) = 1 - \Omega_m(N) = 1 - \frac{\Omega_m^{(0)} e^{-3N(w_m+1)}}{E^2}. \quad (22)$$

Defining  $Z = E^2$ , we obtain the equation

$$Z' = -3(w_m + 1)\Omega_m^{(0)} e^{-3N(w_m+1)} + 2\mathcal{X}Z, \quad Z(0) = 1, \quad (23)$$

where

$$\begin{aligned} \mathcal{X}Z &= -\left[ \left( \Omega_m^{(0)} e^{-3N(w_m+1)} - Z \right)^2 - \frac{4\beta^2 c^2}{3} \right]^{1/2} \\ &\quad + \left[ \frac{2\beta^2 \left( Z - \Omega_m^{(0)} e^{-3N(w_m+1)} \right)^2 - \frac{8\beta^4 c^2}{3}}{3Z^2 - 3Z\Omega_m^{(0)} e^{-3N(w_m+1)} - Z\sqrt{9\left( Z - \Omega_m^{(0)} e^{-3N(w_m+1)} \right)^2 - 12\beta^2 c^2}} \right]^{1/2}. \end{aligned} \quad (24)$$

Thus, the evolution of  $E^2(z)$  can be obtained by substituting (24) into (23). More precisely, substituting (24) into (23), integrating, and imposing the initial condition  $Z(0) = 1$ , gives  $E^2(N)$ . In order to express it as  $E^2(z)$ , we use the relation  $N = \ln(a/a_0) = -\ln(1+z)$ , which is a relation between the e-folding ( $N$ ), the scale factor ( $a$ ), and the redshift ( $z$ ).

Additionally, we can now write the deceleration parameter  $q(z)$ , and a cosmographic parameter which is related to the third-order derivative of the scale factor, i.e. the cosmographic jerk parameter  $j(z)$ , which are given by the formulas

$$q := -1 - \frac{E'}{E}, \quad (25)$$

$$j := q(2q + 1) - q', \quad (26)$$

where  $j = 1$  corresponds to the case of a cosmological constant.

Hence, equation (25) becomes

$$q = -1 + \frac{3}{2}(w_m + 1)(1 - \Omega_{DE}) - \mathcal{X}, \quad (27)$$

with  $X$  defined by (19).  $j$  is found by direct evaluation of (26). We have mentioned before that taking the limit  $\beta \rightarrow 0$  in (17) and (18), and neglecting error terms  $O(\beta^2)$ , we acquire the approximated differential equations

$$\Omega'_{DE} = \frac{\Omega_{DE}(1 - \Omega_{DE})(3w_m c + c + 2\sqrt{\Omega_{DE}})}{c}, \quad (28)$$

$$E' = \frac{E \left\{ 2\Omega_{DE}^{3/2} + c[3w_m(\Omega_{DE} - 1) + \Omega_{DE} - 3] \right\}}{2c}. \quad (29)$$

Equations (28) and (29) characterize standard holographic cosmology. Imposing the conditions

$$E(\Omega_{DE}^{(0)}) = 1, \quad \ln\left(\frac{a}{a_0}\right)\Big|_{\Omega_{DE}^{(0)}} = 0, \quad (30)$$

we obtain the implicit solutions

$$E = \left(\frac{\Omega_{DE}}{\Omega_{DE}^{(0)}}\right)^{-\frac{3(w_m+1)}{6w_m+2}} \left(\frac{1-\sqrt{\Omega_{DE}}}{1-\sqrt{\Omega_{DE}^{(0)}}}\right)^{\frac{c-1}{3cw_m+c+2}} \left(\frac{\sqrt{\Omega_{DE}+1}}{\sqrt{\Omega_{DE}^{(0)}+1}}\right)^{\frac{c+1}{3cw_m+c-2}} \\ \times \left(\frac{3cw_m+c+2\sqrt{\Omega_{DE}}}{3cw_m+c+2\sqrt{\Omega_{DE}^{(0)}}}\right)^{-\frac{12(w_m+1)}{(3w_m+1)(3cw_m+c)^2-4}}, \quad (31)$$

and

$$(1+z)^{-1} := \left(\frac{a}{a_0}\right) \\ = \left(\frac{\Omega_{DE}}{\Omega_{DE}^{(0)}}\right)^{\frac{1}{3w_m+1}} \left(\frac{1-\sqrt{\Omega_{DE}}}{1-\sqrt{\Omega_{DE}^{(0)}}}\right)^{-\frac{c}{3cw_m+c+2}} \left(\frac{\sqrt{\Omega_{DE}+1}}{\sqrt{\Omega_{DE}^{(0)}+1}}\right)^{-\frac{c}{3cw_m+c-2}} \\ \times \left(\frac{3cw_m+c+2\sqrt{\Omega_{DE}}}{3cw_m+c+2\sqrt{\Omega_{DE}^{(0)}}}\right)^{\frac{8}{(3w_m+1)(3cw_m+c)^2-4}}. \quad (32)$$

Lastly, expanding around  $\beta = 0$  and  $\Omega_{DE} = 1$  and removing second order terms, the deceleration parameter (25) and the cosmographic jerk parameter (26) (in the dark-energy dominated epoch) are given by

$$q = -\frac{1}{c} + \frac{(1 - \Omega_{DE})(3cw_m + c + 3)}{2c}, \quad (33)$$

$$j = \frac{2-c}{c^2} + \frac{(1 - \Omega_{DE})(3cw_m + c + 3)[c(3w_m + 2) - 2]}{2c^2}. \quad (34)$$

Furthermore, expanding around  $\beta = 0$  and  $\Omega_{DE} = 0$  and removing second order terms, the deceleration parameter (25) and the cosmographic jerk parameter (26) (in the matter dominated epoch) are given by

$$q = \frac{1}{2}(3w_m + 1)(1 - \Omega_{DE}), \quad (35)$$

$$j = \frac{1}{2}[9w_m(w_m + 1) + 2](1 - \Omega_{DE}). \quad (36)$$

### 3 OBSERVATIONAL ANALYSIS

One of the goals of this work is to provide observational bounds on the parameter of Kaniadakis entropy  $K$  or, more conveniently  $\beta$ , however we are also interested in the behavior of all cosmological parameters, namely on the vector  $\Theta = \{h, \Omega_m^{(0)}, \beta, c\}$ . For the parameter estimation we use the recent measurements of the observational Hubble data as well as data from type Ia supernovae, and baryon acoustic oscillations observations. In what follows, we first briefly introduce these datasets and the Bayesian methodology, and then we apply it in the scenario of Kaniadakis-holographic dark energy, providing the resulting observational constraints.

### 3.1 Data and methodology

#### 3.1.1 Cosmic chronometer data

The Hubble parameter  $H(z)$  describes the expansion rate of the Universe as a function of redshift  $z$ . Currently, this parameter can be estimated from baryon acoustic oscillations measurements and differential age in passive galaxies (dubbed as cosmic chronometers). While the former could be biased due to the assumption of a fiducial cosmology, the samples from cosmic chronometers are independent from the underlying cosmological model. Thus, in this work we only consider the 31 points from cosmic chronometer sample presented in Moresco et al. (2016); Magaña et al. (2018) in the redshift range  $0.07 < z < 1.965$ . We assume a Gaussian likelihood function for this observation as  $\mathcal{L}_{CC} \propto \exp(-\chi_{CC}^2/2)$ , where the figure-of-merit is

$$\chi_{CC}^2 = \sum_i^{31} \left[ \frac{H_{mod}(\Theta, z_i) - H_{dat}(z_i)}{\sigma_{dat}^i} \right]^2, \quad (37)$$

where  $H_{dat}(z_i)$  and  $\sigma_{obs}^i$  are the measured Hubble parameter and its observational uncertainty at the redshift  $z_i$ , respectively. The predicted Hubble parameter by the Kaniadakis-holographic dark energy is denoted by  $H_{mod}(\Theta)$ , and it can be obtained by solving the system of equations (17)-(19).

#### 3.1.2 Pantheon SNIa sample

Since the discovery of the late cosmic acceleration with the observations of high redshift type Ia supernovae (SNIa) by Riess et al. (1998); Perlmutter et al. (1999), the observation of these distant objects is a crucial test to determine if a cosmological scenario is a viable candidate for the description of the late-time Universe. The probe consists of confronting the observed luminosity distance (or distance module) of SNIa with the theoretical prediction of any model. Up to now, the Pantheon sample (Scolnic et al. 2018) is the largest collection of high-redshift SNIa, with 1048 data points with measured redshifts in the range  $0.001 < z < 2.3$ . The authors also provide a binned sample containing 40 points of binned distances  $\mu_{dat,bin}$  in the redshift range  $0.014 < z < 1.61$ . In this work, we use the binned set and we consider a Gaussian likelihood  $\mathcal{L}_{SNIa} \propto \exp(-\chi_{SNIa}^2/2)$ . By marginalizing the nuisance parameters, the figure-of-merit function  $\chi_{SNIa}^2$  is given by

$$\chi_{SNIa}^2 = a + \log\left(\frac{e}{2\pi}\right) - \frac{b^2}{e}, \quad (38)$$

where  $a = \Delta\tilde{\mu}^T \cdot C_P^{-1} \cdot \Delta\tilde{\mu}$ ,  $b = \Delta\tilde{\mu}^T \cdot C_P^{-1} \cdot \Delta\mathbf{1}$ ,  $e = \Delta\mathbf{1}^T \cdot C_P^{-1} \cdot \Delta\mathbf{1}$ , and  $\Delta\tilde{\mu}$  is the vector of residuals between the model distance modulus and the observed (binned) one. The covariance matrix  $C_P$  takes into account systematic and statistical uncertainties (Scolnic et al. 2018). Moreover, the theoretical counterpart of the distance modulus for any cosmological model is given by  $\mu_{mod}(\Theta, z) = 5 \log_{10}(d_L(\Theta, z)/10\text{pc})$ , where  $d_L$  is the luminosity distance given by

$$d_L(\Theta, z) = \frac{\tilde{c}}{H_0} (1+z) \int_0^z \frac{dz'}{E(z')}, \quad (39)$$

where  $\tilde{c}$  is the light speed.

#### 3.1.3 Baryon Acoustic Oscillations

Baryon Acoustic Oscillations (BAO) are fluctuation patterns in the matter density field as result of internal interactions in the hot primordial plasma during the pre-recombination stage. Based on luminous

red galaxies, a sample of 15 transversal BAO scale measurements within the redshift  $0.110 < z < 2.225$  were collected by Nunes et al. (2020). Assuming a Gaussian likelihood,  $\mathcal{L}_{\text{BAO}} \propto \exp(-\chi_{\text{BAO}}^2/2)$ , we build the figure of merit function as

$$\chi_{\text{BAO}}^2 = \sum_{i=1}^{15} \left[ \frac{\theta_{\text{dat}}^i - \theta_{\text{mod}}(\Theta, z_i)}{\sigma_{\theta_{\text{dat}}^i}} \right]^2, \quad (40)$$

where  $\theta_{\text{dat}}^i \pm \sigma_{\theta_{\text{dat}}^i}$  is the BAO angular scale and its uncertainty at 68% measured at  $z_i$ . The theoretical BAO angular scale counterpart, denoted as  $\theta_{\text{mod}}$ , is estimated by

$$\theta_{\text{mod}}(z) = \frac{r_{\text{drag}}}{(1+z)D_A(z)}, \quad (41)$$

where  $D_A = d_L(z)/(1+z)^2$  is the angular diameter distance at  $z$  which depends on the dimensionless luminosity distance  $d_L(z)$ , and  $r_{\text{drag}}$  is the sound horizon at the baryon drag epoch, considered to be  $r_{\text{drag}} = 137.7 \pm 3.6$  Mpc (Aylor et al. 2019).

### 3.1.4 Bayesian analysis

A Bayesian statistical analysis based on Markov Chain Monte Carlo (MCMC) algorithm is performed to bound the free parameters of the Kaniadakis-holographic dark energy. The MCMC approach is implemented through the emcee python module (Foreman-Mackey et al. 2013) in which we generate 1000 chains with 250 steps, each one after a burn-in phase. The latter is stopped when the chains have converged based on the auto-correlation time criteria. Thus, the inference of the parameter space is obtained by minimizing a Gaussian log-likelihood,  $-2 \ln(\mathcal{L}_{\text{data}}) \propto \chi_{\text{data}}^2$ , considering flat priors in the intervals:  $h \in [0.2, 1]$ ,  $\Omega_m^{(0)} \in [0, 1]$ ,  $\beta \in [-1, 1]$ ,  $c \in [0, 2]$  for each dataset. Additionally, a combined analysis is performed by assuming no correlation between the datasets, hence the figure of merit is

$$\chi_{\text{Joint}}^2 = \chi_{\text{CC}}^2 + \chi_{\text{SNIa}}^2 + \chi_{\text{BAO}}^2, \quad (42)$$

namely, the sum of the  $\chi^2$  corresponding to each sample as previously defined.

## 3.2 Results from observational constraints

We perform the full confrontation described above for the scenario of Kaniadakis holographic dark energy, and in Fig. 1 we present the 2D parameter likelihood contours at 68% (1 $\sigma$ ) and 99.7% (3 $\sigma$ ) confidence level (CL) respectively, alongside the corresponding 1D posterior distribution of the parameters. Additionally, Table 1 shows the mean values of the parameters and their uncertainties at 1 $\sigma$ .

In order to statistically compare these results with  $\Lambda$ CDM cosmology, we apply the corrected Akaike information criterion (AICc) (Akaike 1974; Sugiura 1978; Hurvich & Tsai 1989) and the Bayesian information criterion (BIC) (Schwarz 1978). They give a penalty according to size of data sample ( $N$ ) and the number of degrees of freedom ( $k$ ) defined as  $\text{AICc} = \chi_{\text{min}}^2 + 2k + (2k^2 + 2k)/(N - k - 1)$  and  $\text{BIC} = \chi_{\text{min}}^2 + k \log(N)$  respectively, where  $\chi_{\text{min}}^2$  is the minimum value of the  $\chi^2$ . Thus, a model with lower values of AICc and BIC is preferred by the data. According to the difference between a given model and the reference one, denoted as  $\Delta\text{AICc}$ , one has the following: if  $\Delta\text{AICc} < 4$ , both models are supported by the data equally, i.e they are statistically equivalent. If  $4 < \Delta\text{AICc} < 10$ , the data still support the given model but less than the preferred one. If  $\Delta\text{AICc} > 10$ , it indicates that the data does not support the given model. Similarly, the difference between a candidate model and the reference model,

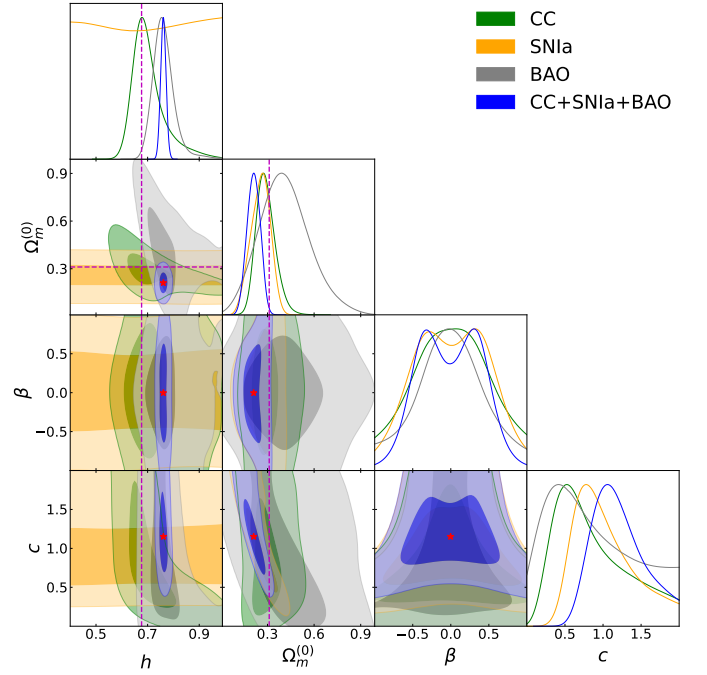


**Figure 1.** Two-dimensional likelihood contours at 68% and 99.7% confidence level (CL), alongside the corresponding 1D posterior distribution of the free parameters, in Kaniadakis-holographic dark energy case. The stars denote the mean values using the joint analysis, and the dashed lines represent the best-fit values for  $\Lambda$ CDM cosmology (Aghanim et al. 2020).

denoted as  $\Delta\text{BIC}$ , is interpreted in this way: if  $\Delta\text{BIC} < 2$ , there is no evidence against the candidate model, if  $2 < \Delta\text{BIC} < 6$ , there is modest evidence against the candidate model, if  $6 < \Delta\text{BIC} < 10$ , there is strong evidence against the candidate model, and  $\Delta\text{BIC} > 10$  gives the strongest evidence against it. Hence, we have performed the above comparison, taking  $\Lambda$ CDM scenario as the reference model, and we display the results in the last two columns of Table 1.

A first observation is that the Kaniadakis parameter  $\beta$  is constrained around 0 as expected, namely around the value in which Kaniadakis entropy recovers the standard Bekenstein-Hawking one. A second observation is that the scenario at hand gives a slightly smaller value for  $\Omega_m^{(0)}$  comparing to  $\Lambda$ CDM cosmology, however it estimates a higher value for the present Hubble constant  $h$ , closer to its direct measurements through long-period Cepheids. In particular, it is consistent within 1 $\sigma$  with the value reported by Riess et al. (2019) and it exhibits a deviation of 4.18 $\sigma$  from the one obtained by Planck Aghanim et al. (2020). On the other hand, based on our mean value of  $c = 1.151^{+0.401}_{-0.287}$  it is interesting that we do not observe a turning point in the  $H(z)$  reconstruction shown in Fig. 2, a feature from which the usual holographic dark energy suffers when  $c < 1$  (Colgáin & Sheikh-Jabbari 2021). Hence, we deduce that Kaniadakis holographic dark energy can also solve such a problem and thus avoid to violate the Null Energy Condition (NEC).

Concerning the comparison with  $\Lambda$ CDM scenario, for the combined dataset analysis we find that  $\Delta\text{AICc}$  implies that  $\Lambda$ CDM is strongly favored over Kaniadakis-holographic dark energy. This result is also supported by BIC, for which  $\Delta\text{BIC}$  gives a strong evidence against it. Notice that these comparisons were performed by using the same datasets for both models  $\Lambda$ CDM and Kaniadakis cosmology.

Finally, based on the combined (CC+SNIa+BAO) analysis, in Fig. 2 we present the reconstruction of the Hubble parameter  $H(z)$ ,

**Table 1.** Mean values of various parameters and their 68% CL uncertainties for Kaniadakis-holographic dark energy. The quantities  $\Delta\text{AICc}$  ( $\Delta\text{BIC}$ ) are the differences with respect to  $\Lambda\text{CDM}$  paradigm.

Sample	$\chi^2$	$h$	$\Omega_m^{(0)}$	$\beta$	$c$	$\Delta\text{AICc}$	$\Delta\text{BIC}$
CC	14.69	$0.690^{+0.072}_{-0.043}$	$0.284^{+0.066}_{-0.055}$	$0.012^{+0.486}_{-0.489}$	$0.729^{+0.665}_{-0.350}$	5.2	7.0
SNIa	48.52	$0.597^{+0.279}_{-0.271}$	$0.259^{+0.059}_{-0.069}$	$0.013^{+0.480}_{-0.482}$	$0.932^{+0.492}_{-0.302}$	5.1	7.5
BAO	13.01	$0.758^{+0.041}_{-0.035}$	$0.403^{+0.167}_{-0.151}$	$-0.006^{+0.433}_{-0.418}$	$0.756^{+0.759}_{-0.463}$	8.2	5.6
CC+SNIa+BAO	98.07	$0.761^{+0.011}_{-0.010}$	$0.211^{+0.043}_{-0.044}$	$-0.003^{+0.412}_{-0.420}$	$1.151^{+0.401}_{-0.287}$	21.7	26.1

the deceleration parameter  $q(z)$  (equation (25)), and the cosmographic jerk parameter  $j(z)$  (equation (26)), in the redshift range  $0 < z < 2$ . For comparison, we also depict the corresponding curves for  $\Lambda\text{CDM}$  scenario. Concerning the current values, our analysis leads to  $H_0 = 76.09^{+1.06}_{-1.02}$  km/s/Mpc,  $q_0 = -0.537^{+0.064}_{-0.064}$ ,  $j_0 = 0.815^{+0.315}_{-0.274}$ , where the uncertainties correspond to  $1\sigma$  CL. Additionally, using the joint analysis we find the redshift for the deceleration-acceleration transition as  $z_T = 0.860^{+0.213}_{-0.138}$ , and the Universe age as  $t_U = 13.000^{+0.406}_{-0.350}$  Gyrs. Notice that  $z_T$  value is in agreement within  $1\sigma$  with the value reported in [Herrera-Zamorano et al. \(2020\)](#) for  $\Lambda\text{CDM}$  paradigm ( $z_T = 0.642^{+0.014}_{-0.014}$ ).

#### 4 DYNAMICAL SYSTEM AND STABILITY ANALYSIS

In this section we apply the powerful method of phase-space and stability analysis, which allows us to obtain a qualitative description of the local and global dynamics of cosmological scenarios, independently of the initial conditions and the specific evolution of the universe. The extraction of asymptotic solutions give theoretical values that can be compared with the observed ones, such as the dark-energy and total equation-of-state parameters, the deceleration parameter, the density parameters of the different sectors, etc., and also allows the classification of the cosmological solutions ([Wainwright & Ellis 1997](#)).

In order to perform the stability analysis of a given cosmological scenario, one transforms it to its autonomous form  $\mathbf{X}' = \mathbf{f}(\mathbf{X})$  ([Wainwright & Ellis 1997](#); [Ferreira & Joyce 1997](#); [Copeland et al. 1998](#); [Perko 2000](#); [Coley 2003](#); [Copeland et al. 2006](#); [Chen et al. 2009](#); [Cotsakis & Kittou 2013](#); [Giambo & Miritzis 2010](#)), where  $\mathbf{X}$  is the column vector containing the auxiliary variables and primes denote derivative with respect to a conveniently chosen time variable. Then, one extracts the critical points  $\mathbf{X}_c$  by imposing the condition  $\mathbf{X}' = 0$  and, to determine their stability properties, one expands around them with  $\mathbf{U}$  the column vector of the perturbations of the variables. Therefore, for each critical point the perturbation equations are expanded to first order as  $\mathbf{U}' = \mathbf{Q} \cdot \mathbf{U}$ , with the matrix  $\mathbf{Q}$  containing the coefficients of the perturbation equations. Finally, the eigenvalues of  $\mathbf{Q}$  determine the type and stability of the critical point under consideration.

##### 4.1 Local dynamical system formulation

In this subsection we study the stability of system (17)-(18) with  $X$  defined in (19), in the phase space

$$\left\{ (E, \Omega_{DE}) \in \mathbb{R}^2 : 3E^4 \Omega_{DE}^2 - 4\beta^2 c^2 \geq 0 \right\}. \quad (43)$$

For generality, we keep the matter equation-of-state parameter  $w_m$  in the calculations, and it can be set to zero in the final result if needed. Since  $\beta$  and  $c$  appear quadratic in (17), (18) (19) and (43), these equations are invariant under the changes  $c \mapsto -c$  and  $\beta \mapsto -\beta$ .

Therefore, in this section we focus on  $\beta > 0$  and  $c > 0$ . When  $\beta < 0$  we change  $\beta$  by  $-\beta$  and  $c$  by  $-c$  on the next discussion.

The equilibrium points dominated by dark energy (namely possessing  $\Omega_{DE} = 1$ ) with finite  $H$  are:

- $L_1 : (E, \Omega_{DE}) = \left( \frac{\sqrt{2\beta c}}{\sqrt[4]{3}}, 1 \right)$ . This point always satisfies  $-12c^2\beta^2 + 9E^4\Omega_{DE}^2 = 0$ . The eigenvalues are  $\left\{ -3(w_m + 1), \infty \operatorname{sgn} \left( (\sqrt{2} - 2c) \right) \right\}$ . It is a stable point for  $c > \frac{\sqrt{2}}{2}$  and  $w_m > -1$ , and a saddle for  $c < \frac{\sqrt{2}}{2}$  and  $w_m > -1$ .

- $L_2 : (E, \Omega_{DE}) = \left( \frac{\sqrt{\beta}}{\sqrt[4]{3(1-c^2)}}, 1 \right)$ . This point satisfies the reality condition if  $\frac{3\beta^2(1-2c^2)^2}{1-c^2} \geq 0$ , namely  $\beta = 0, c^2 > 1$  or  $\beta \neq 0, c^2 < 1$ . For  $c^2 \leq \frac{1}{2}$  the eigenvalues are

$$\lambda_{1,2} = \left\{ \frac{(4c^4 - 4c^2 - 1)|c| + (-8c^4 + 6c^2 + 1)\sqrt{1-c^2}}{|c - 2c^3|}, 2 \left( \sqrt{\frac{1}{c^2} - 1} - 1 \right) (2c^2 - 1) - 3(w_m + 1) \right\}.$$

This is a saddle point, as it can be verified numerically in [Fig. 3](#). Moreover, for  $\frac{1}{2} < c^2 < 1$ , the eigenvalues are  $\{2 - 2c^2, -3(w_m + 1)\}$ , and thus for  $w_m > -1$  it is also a saddle point.

Since  $\Omega_{DE}^2 \geq \frac{4\beta^2 c^2}{3E^4} \geq 0$ , we deduce that the only possibility to have matter domination, namely  $\Omega_{DE} = 0$ , is when  $E \rightarrow \infty$ , due to the reality condition  $c^2\beta^2 \geq 0$ . It is convenient to define the dimensionless compact variable  $T = (1 + E)^{-1}$  such that  $T \rightarrow 0$  as  $E \rightarrow \infty$  and  $T \rightarrow 1$  as  $E \rightarrow 0$ . Then, we obtain

$$T' = \frac{3}{2}(T-1)T(w_m+1)(\Omega_{DE}-1) - \frac{T^3 \sqrt{\frac{(T-1)^4 \Omega_{DE}^2 - 4\beta^2 c^2}{T^4}}}{T-1} - \frac{T^5 \sqrt{\frac{2\beta^2 (T-1)^4 \Omega_{DE}^2 - 8\beta^4 c^2}{T^4}}}{(T-1)^2 \sqrt{3(T-1)^2 \Omega_{DE} - \sqrt{9(T-1)^4 \Omega_{DE}^2 - 12\beta^2 c^2 T^4}}}, \quad (44)$$

$$\Omega'_{DE} = (\Omega_{DE} - 1) \left[ -3(w_m + 1)\Omega_{DE} + \frac{2T^2 \sqrt{\frac{(T-1)^4 \Omega_{DE}^2 - 4\beta^2 c^2}{T^4}}}{(T-1)^2} + \frac{2T^2 \sqrt{2\beta^2 (T-1)^4 \Omega_{DE}^2 - \frac{8}{3}\beta^4 c^2 T^4}}{(T-1)^3 \sqrt{3(T-1)^2 \Omega_{DE} - \sqrt{9(T-1)^4 \Omega_{DE}^2 - 12\beta^2 c^2 T^4}}} \right], \quad (45)$$

defined on the physical region

$$9(T-1)^4 \Omega_{DE}^2 - 12\beta^2 c^2 T^4 \geq 0. \quad (46)$$

In summary the sources/sinks are:

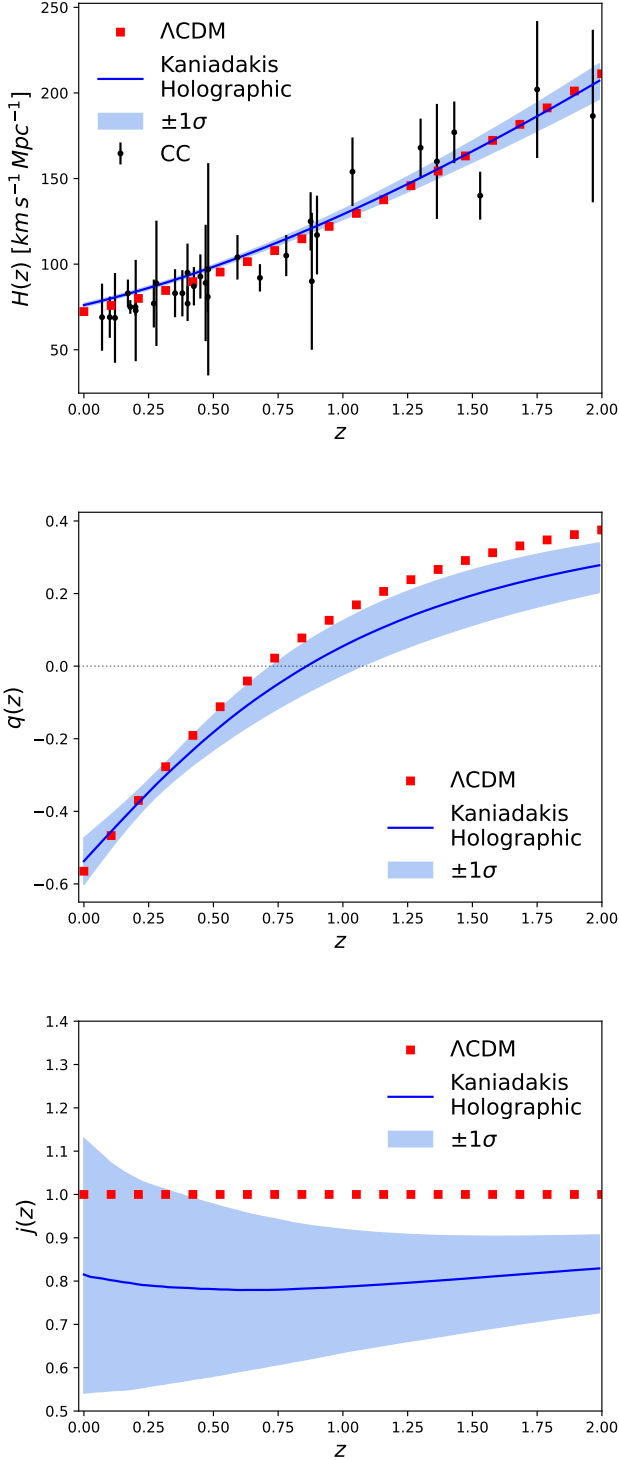


**Figure 2.** Reconstruction of the Hubble function ( $H(z)$ , upper panel), the deceleration parameter ( $q(z)$ , middle panel), and the jerk parameter ( $j(z)$ , bottom panel) for the Kaniadakis-holographic dark energy using the combined (CC+SNIa+BAO) analysis in the redshift range  $0 < z < 2$ . The shaded regions represent the 68% confidence level, and the square points depict the results of the  $\Lambda$ CDM scenario with  $h = 0.723$  and  $\Omega_m^{(0)} = 0.290$ , namely the values obtained through observational confrontation using the same datasets with the analysis of Kaniadakis holographic dark energy.

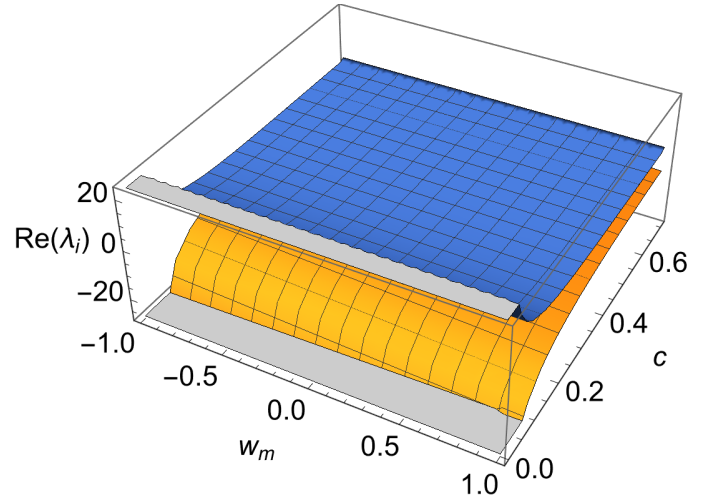


**Figure 3.** The eigenvalues corresponding to the point  $L_2$ , for  $w_m \in [-1, 1]$ ,  $c \in [0, \sqrt{2}/2]$ .

- $L_1 : (E, \Omega_{DE}) = \left( \frac{\sqrt{2\beta c}}{\sqrt{3}}, 1 \right)$  is a stable point for  $c > \frac{\sqrt{2}}{2}$  and  $w_m > -1$ , and a saddle for  $c < \frac{\sqrt{2}}{2}$  and  $w_m > -1$ .
- For the dark-energy dominated solution  $L_3 : (T, \Omega_{DE}) = (0, 1)$ , the eigenvalues are  $\left\{ \frac{c-1}{c}, -\frac{3cw_m+c+2}{c} \right\}$ , thus it is a stable point for  $-1 < w_m < 1$  and  $0 < c < 1$  or a saddle for  $-1 < w_m < 1$  and  $c > 1$ .
- The past attractor is the matter dominated solution  $L_4 : (T, \Omega_{DE}) = (0, 0)$ , for which the eigenvalues are  $\left\{ 3(w_m + 1), \frac{3(w_m+1)}{2} \right\}$ , and since they are always positive for  $-1 < w_m < 1$  it is an unstable point.

We remark here that  $E = E_c$  finite corresponds to the de Sitter solution with  $H = E_c H_0$ , and  $a(t) \propto e^{E_c H_0 t}$ . That is, point  $L_1$  satisfies  $a(t) \propto e^{\frac{\sqrt{2\beta c}}{\sqrt{3}} H_0 t}$  and it is a late-time attractor providing the accelerated regime. Additionally, for  $\beta \neq 0$ ,  $c^2 < 1$ , the point  $L_2$  exists and satisfies  $a(t) \propto e^{\frac{\sqrt{\beta}}{\sqrt{3(1-c^2)}} H_0 t}$ , and since it is a saddle it can provide a transient accelerated phase that can be related to inflation.

In order to present the results in a more transparent way, in Fig. 4 we show a phase-space plot of the system (44)-(45) for the best fit values  $\beta = -0.003$  and  $c = 1.151$  and for dust matter ( $w_m = 0$ ). The red curve represents the solution for the initial data  $\Omega_{DE}|_{z=0} = 0.71$ , corresponding to the mean value from the joint analysis CC+SNIa+BAO, and for  $T|_{z=0} = 0.5$ . The dashed blue region is the physical region  $9(T-1)^4 \Omega_{DE}^2 - 12\beta^2 c^2 T^4 \geq 0$ , where the equations are real-valued. From this figure it is confirmed that the late-time attractor is the dark-energy dominated solution  $\Omega_{DE} = 1$  with  $T = 0$ . The past attractor is the matter-dominated solution  $\Omega_{DE} = 0$  with  $T = 0$ . At the finite region, point  $L_1$  is the stable one.

Setting  $\Omega_{DE} = 1$ , the system (44)-(45) becomes a one-dimensional dynamical system:

$$T' = \frac{T^3 \sqrt{\frac{(T-1)^4}{T^4} - \frac{4\beta^2 c^2}{3}}}{1-T} - \frac{T^3 \sqrt{2\beta^2 (T-1)^4 - \frac{8}{3}\beta^4 c^2 T^4}}{(T-1)^2 \sqrt{3(T-1)^2 - \sqrt{9(T-1)^4 - 12\beta^2 c^2 T^4}}}. \quad (47)$$

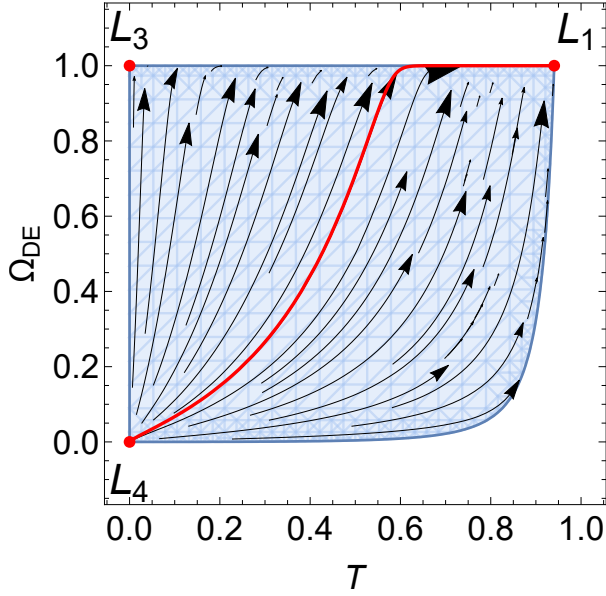


**Figure 4.** Phase-space plot of the dynamical system (44)-(45), for the best fit values  $\beta = -0.003$  and  $c = 1.151$  of Kaniadakis-holographic dark energy, and for dust matter ( $w_m = 0$ ). The red curve represents the solution for the initial data  $\Omega_{DE}|_{z=0} = 0.71$ , corresponding to the mean value from the joint analysis CC+SNIa+BAO, and for  $T|_{z=0} = 0.5$ . The dashed blue region is the physical region  $9(T-1)^4\Omega_{DE}^2 - 12\beta^2c^2T^4 \geq 0$ , where the equations are real-valued.

The origin  $T = 0$  has eigenvalue  $\lambda = 1 - \frac{1}{|c|}$ . Moreover, the system admits, at most, four additional equilibrium points  $T_c$ , with  $T_c \in \{T_1, T_2, T_3, T_4\}$  satisfying  $\frac{(T-1)^4}{T^4} - \frac{4\beta^2c^2}{3} = 0$ . Explicitly, we have that

$$T_{1,2} = \frac{3}{3 - 4\beta^2c^2} - \frac{2\sqrt{3}|c\beta|}{|3 - 4c^2\beta^2|} \pm \frac{\sqrt{2}\sqrt{12|c\beta||3 - 4c^2\beta^2| + \sqrt{3}(16\beta^4c^4 - 9)}\sqrt{|c\beta|}}{|3 - 4c^2\beta^2|^{3/2}},$$

$$T_{3,4} = \frac{3}{3 - 4\beta^2c^2} + \frac{2\sqrt{3}|c\beta|}{|3 - 4c^2\beta^2|} \quad (48a)$$

$$\pm \frac{\sqrt{2}\sqrt{12|c\beta||3 - 4c^2\beta^2| + \sqrt{3}(9 - 16\beta^4c^4)}\sqrt{|c\beta|}}{|3 - 4c^2\beta^2|^{3/2}}. \quad (48b)$$

Such points with  $0 < T_c < 1$ , corresponding to de Sitter solution  $a(t) \propto e^{H_0 t (\frac{1}{T_c} - 1)}$ , are stable for  $c \geq 1$  and otherwise are saddle.

For the best-fit values  $\beta = -0.003$  and  $c = 1.151$ , the origin has eigenvalue  $\lambda \approx 0.13$ , and therefore it is a source. In this case the only real value is  $T_3 \approx 0.941$ . The exact eigenvalue is negative infinity (for  $c \geq 1$ ) at the exact value of  $T_3$ , and therefore it is stable. In Fig. 5 we draw a phase-space plot of the one-dimensional dynamical system (47), for the best fit values  $\beta = -0.003$  and  $c = 1.151$  of Kaniadakis holographic dark energy. The equilibrium point  $T = 0$  is unstable, while the de Sitter equilibrium point  $T = T_c \approx 0.941$  is stable.

## 4.2 Global dynamical systems formulation

In the previous subsection we performed the local analysis of the scenario. However, due to the presence of rational functions that are

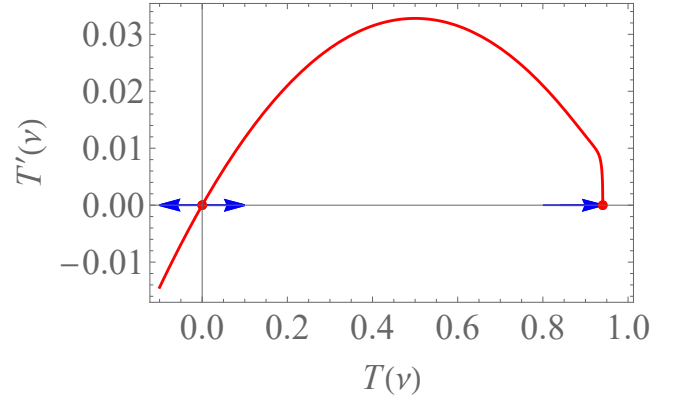


**Figure 5.** Phase-space plot of the one-dimensional dynamical system (47), for the best fit values  $\beta = -0.003$  and  $c = 1.151$  of Kaniadakis-holographic dark energy. The equilibrium point  $T = 0$  is unstable, while the de Sitter equilibrium point  $T = T_c \approx 0.941$  is stable.

not analytic in the whole domain, it becomes necessary to investigate the full global dynamics. We start by defining the dimensionless variables  $\theta, T$  as

$$T = \frac{H_0}{H + H_0} = \frac{1}{1 + E}, \quad \theta = \arcsin\left(\sqrt{1 - \frac{\rho_{DE}}{3M_p^2 H^2}}\right), \quad (49)$$

such that

$$\sin^2(\theta) = \frac{\rho_m}{3M_p^2 H^2}, \quad \cos^2(\theta) = \frac{\rho_{DE}}{3M_p^2 H^2}. \quad (50)$$

For an expanding universe ( $H > 0$ ), we have that  $T \in [0, 1]$ , while  $\theta$  is a periodic coordinate and, thus, we can set  $\theta \in [-\pi, \pi]$ . Therefore, we obtain a global phase-space formulation.

### 4.2.1 Standard holographic dark energy ( $\beta = 0$ )

In order to present the features of Kaniadakis-holographic dark energy in comparison with standard-holographic dark energy, we first analyze the latter case for completeness, namely we consider the system (28)-(29) for  $\beta = 0$ . In this case, we obtain

$$T' = \frac{(T-1)T \{ \cos^2(\theta)[(3w_m + 1)c + 2 \cos(\theta)] - 3c(w_m + 1) \}}{2c}, \quad (51)$$

$$\theta' = -\frac{[(3w_m + 1)c + 2 \cos(\theta)] \sin(2\theta)}{4c}. \quad (52)$$

The critical points of the above system, alongside their associated eigenvalues, are presented in Table 2. Note that  $\theta$  is unique modulo  $2\pi$ , and focus on  $\cos \theta \geq 0$ . In the following list  $\arctan[x, y]$  gives the arc tangent of  $y/x$ , taking into account on which quadrant the point  $(x, y)$  is in. When  $x^2 + y^2 = 1$ ,  $\arctan[x, y]$  gives the number  $\theta$  such that  $x = \cos \theta$  and  $y = \sin \theta$ .

In summary, in the case  $\beta = 0$ , the critical points can be completely characterized. In particular:

- Point  $P_1$  always exists. It corresponds to a dark-energy dominated solution, i.e.  $\Omega_{DE} = 1$  with  $T = 0$ . It is a stable point for  $-1 < w_m < 1$ ,  $0 < c < 1$ .
- Points  $P_2$  and  $P_3$  exist always. They are two representations of the matter-dominated solution  $\Omega_{DE} = 0$  with  $T = 0$ . They are past attractors, i.e. unstable points, for  $-\frac{1}{3} < w_m \leq 1$ , while they are saddle for  $-1 < w_m < -\frac{1}{3}$ .

**Table 2.** The critical points and their associated eigenvalues of the system (51)-(52) for  $\beta = 0$  in (28)-(29), namely for the case of standard holographic dark energy. We use the notation  $x = \frac{1}{2}c(3w_m + 1)$ , while  $c_1 \in \mathbb{Z}$ .

Label	$(T, \theta)$	Eigenvalues
$P_1$	$(0, 2\pi c_1)$	$\left\{ \frac{c-1}{c}, -\frac{3w_m c + c + 2}{2c} \right\}$
$P_2$	$\left(0, \frac{1}{2}\pi(4c_1 - 1)\right)$	$\left\{ \frac{3(w_m+1)}{2}, \frac{1}{2}(3w_m + 1) \right\}$
$P_3$	$\left(0, \frac{1}{2}\pi(4c_1 + 1)\right)$	$\left\{ \frac{3(w_m+1)}{2}, \frac{1}{2}(3w_m + 1) \right\}$
$P_4^\pm$	$(0, 2\pi c_1 \pm \pi)$	$\left\{ 1 + \frac{1}{c}, -\frac{3w_m}{2} + \frac{1}{c} - \frac{1}{2} \right\}$
$P_5$	$\left(0, \arctan\left[-x, -\sqrt{1-x^2}\right] + 2\pi c_1\right)$	$\left\{ \frac{3(w_m+1)}{2}, \frac{1}{8}(3w_m + 1)\left(c^2(1+3w_m)^2 - 4\right) \right\}$
$P_6$	$\left(0, \arctan\left[-x, \sqrt{1-x^2}\right] + 2\pi c_1\right)$	$\left\{ \frac{3(w_m+1)}{2}, \frac{1}{8}(3w_m + 1)\left(c^2(1+3w_m)^2 - 4\right) \right\}$
$P_7$	$(1, 2\pi c_1)$	$\left\{ \frac{1}{c} - 1, -\frac{3w_m c + c + 2}{2c} \right\}$
$P_8$	$\left(1, \frac{1}{2}\pi(4c_1 - 1)\right)$	$\left\{ -\frac{3}{2}(w_m + 1), \frac{1}{2}(3w_m + 1) \right\}$
$P_9$	$\left(1, \frac{1}{2}\pi(4c_1 + 1)\right)$	$\left\{ -\frac{3}{2}(w_m + 1), \frac{1}{2}(3w_m + 1) \right\}$
$P_{10}^\pm$	$(1, 2\pi c_1 \pm \pi)$	$\left\{ -\frac{c+1}{c}, -\frac{3w_m}{2} + \frac{1}{c} - \frac{1}{2} \right\}$
$P_{11}$	$\left(1, \arctan\left[-x, -\sqrt{1-x^2}\right] + 2\pi c_1\right)$	$\left\{ -\frac{3}{2}(w_m + 1), \frac{1}{8}(3w_m + 1)\left(c^2(1+3w_m)^2 - 4\right) \right\}$
$P_{12}$	$\left(1, \arctan\left[-x, \sqrt{1-x^2}\right] + 2\pi c_1\right)$	$\left\{ -\frac{3}{2}(w_m + 1), \frac{1}{8}(3w_m + 1)\left(c^2(1+3w_m)^2 - 4\right) \right\}$

- Points  $P_4^\pm$  exist always. They correspond to the dark-energy dominated solution with  $\Omega_{DE} = 1$  with  $T = 0$ . They are unstable points for  $0 < c < \frac{1}{2}$ ,  $-1 \leq w_m \leq 1$ , or  $c \geq \frac{1}{2}$ ,  $-1 \leq w_m < \frac{2-c}{3c}$ , while they are saddle for  $c > \frac{1}{2}$ ,  $\frac{2-c}{3c} < w_m \leq 1$ .

- Points  $P_5$  and  $P_6$  exist for  $-1 \leq \frac{1}{2}c(3w_m + 1) \leq 1$ . They are sources for  $0 \leq c \leq 1$ ,  $-1 < w_m < -\frac{1}{3}$  or  $c > 1$ ,  $-\frac{c+2}{3c} < w_m < -\frac{1}{3}$ . For  $0 \leq c < \frac{1}{2}$ ,  $-\frac{1}{3} < w_m \leq 1$ , or  $c \geq \frac{1}{2}$ ,  $-\frac{1}{3} < w_m < \frac{2-c}{3c}$ , they are saddle.

- Point  $P_7$  exists always. It corresponds to a dark-energy dominated solution  $\Omega_{DE} = 1$  with  $T = 1$ . It is a stable point for  $c > 1$ ,  $-\frac{c+2}{3c} < w_m \leq 1$ .

- Points  $P_8$  and  $P_9$  exist always. They are two representations of the matter-dominated solution  $\Omega_{DE} = 0$  with  $T = 1$ . They are stable points for  $-1 < w_m < -\frac{1}{3}$ , while they are saddle points for  $-\frac{1}{3} < w_m \leq 1$ .

- Points  $P_{10}^\pm$  are two representations of the matter-dominated solution  $\Omega_{DE} = 0$  with  $T = 1$ . They are stable points for  $c > \frac{1}{2}$ ,  $\frac{2-c}{3c} < w_m \leq 1$ , while they are saddle for  $0 < c < \frac{1}{2}$ ,  $-1 \leq w_m \leq 1$ , or  $c \geq \frac{1}{2}$ ,  $-1 \leq w_m < \frac{2-c}{3c}$ .

- Points  $P_{11}$  and  $P_{12}$  exist for  $-1 \leq \frac{1}{2}c(3w_m + 1) \leq 1$ . They are saddle for  $0 \leq c \leq 1$ ,  $-1 < w_m < -\frac{1}{3}$  or  $c > 1$ ,  $-\frac{c+2}{3c} < w_m < -\frac{1}{3}$ , while for  $0 \leq c < \frac{1}{2}$ ,  $-\frac{1}{3} < w_m \leq 1$ , or  $c \geq \frac{1}{2}$ ,  $-\frac{1}{3} < w_m < \frac{2-c}{3c}$ , they are stable.

In order to give a better picture of the system behavior, Fig. 6 display a phase-space plot of the system (51)-(52) for  $\beta = 0$  in (28)-(29), and dust matter. The red curve corresponds to the universe evolution according to parameter mean values from the joint analysis. From this figure we deduce that the late-time attractor is the dark-energy dominated solution with  $\Omega_{DE} = 1$  and  $T = 1$  (point  $P_7$ ), while the past attractor is the matter-dominated solution with  $\Omega_{DE} = 0$  and  $T = 0$  (point  $P_3$ ). For other initial conditions there are other late-time attractors, such as points  $P_{11}$  and  $P_{12}$  which are stable for the best-fit parameters since they satisfy  $c \geq \frac{1}{2}$ ,  $-\frac{1}{3} < w_m < \frac{2-c}{3c}$ . These points are scaling solutions since they have  $\Omega_{DE} = x^2$  and  $\Omega_{DM} = 1 - x^2$ , with  $x = \frac{c}{2}(3w_m + 1) = \frac{c}{2}$  for  $w_m = 0$ . Additionally, points  $P_2, P_3$ , which are matter-dominated solutions, and points  $P_4^\pm$ , which are dark-energy dominated solutions, are also past attractors.

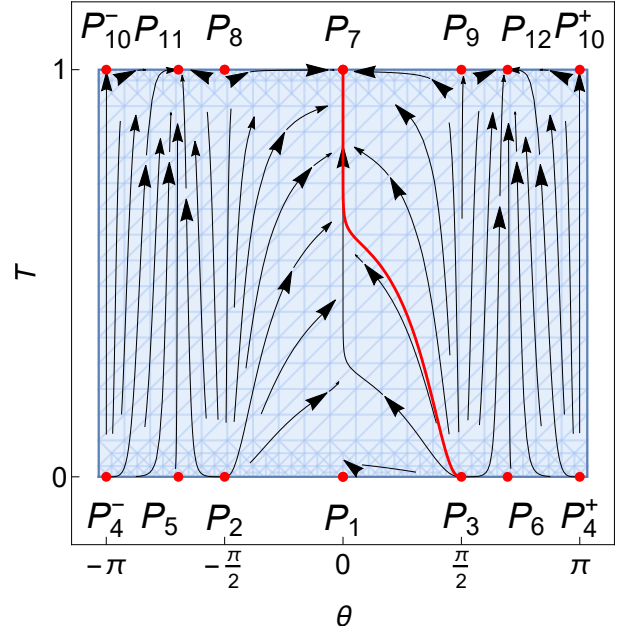


**Figure 6.** Phase-space plot of the dynamical system (51)-(52) for  $\beta = 0$  in (28)-(29), namely for standard holographic dark energy, for the value  $c = 1.151$ , and for dust matter  $w_m = 0$ . The red curve represents the solution for the initial data  $\Omega_{DE}|_{z=0} = 0.71$  (i.e.,  $\theta(0) = \arccos\left(\frac{1}{10}\sqrt{71}\right) \approx 0.569$ ), corresponding to the mean value obtained with the joint analysis CC+SNIa+BAO, and for  $T|_{z=0} = 0.5$ . The dashed blue region is the physical region where the equations are real-valued.

#### 4.2.2 Kaniadakis holographic dark energy ( $\beta \neq 0$ )

Let us now investigate the full extended model of Kaniadakis holographic dark energy, namely the general case where  $\beta \neq 0$ . The full system (17)-(18) becomes

$$T' = \frac{3}{2}(1-T)T(w_m + 1)\sin^2(\theta) + \frac{T^3 \sqrt{\frac{(1-T)^4 \cos^4(\theta) - 4\beta^2 c^2}{T^4}}}{1-T} - \frac{T^5 \sqrt{\frac{18(1-T)^4 \cos^4(\theta)\beta^2}{T^4} - 24\beta^4 c^2}}{3(T-1)^2 \sqrt{3(T-1)^2 \cos^2(\theta) - \sqrt{9(1-T)^4 \cos^4(\theta) - 12\beta^2 c^2 T^4}}}, \quad (53)$$

$$\theta' = -\frac{3}{4}(w_m + 1) \sin(2\theta) + \frac{T^2 \tan(\theta) \sqrt{\frac{(1-T)^4 \cos^4(\theta)}{T^4} - \frac{4\beta^2 c^2}{3}}}{(T-1)^2} - \frac{\sqrt{\frac{2}{3}} T^2 \tan(\theta) \sqrt{-\beta^2 (4\beta^2 c^2 T^4 - 3(1-T)^4 \cos^4(\theta))}}{(1-T)^3 \sqrt{3(1-T)^2 \cos^2(\theta) - \sqrt{9(1-T)^4 \cos^4(\theta) - 12\beta^2 c^2 T^4}}}. \quad (54)$$

Moreover, the physical region of the phase space is

$$3(1-T)^4 \cos^4(\theta) - 4\beta^2 c^2 T^4 \geq 0. \quad (55)$$

We proceed by studying the critical points of the system (53)-(54) in the physical region (55) and their stability. We mention that for  $\beta \neq 0$  the invariant set  $T = 1$  is not physical. Near the invariant set  $T = 0$  the system (53)-(54) becomes

$$T' = \left[ -\frac{\cos^3(\theta)}{c} + \cos^2(\theta) + \frac{3}{2}(w_m + 1) \sin^2(\theta) \right] T + O(T^2), \quad (56)$$

$$\theta' = -\frac{[(3w_m + 1)c + 2 \cos(\theta)] \sin(2\theta)}{4c} + O(T^2). \quad (57)$$

In Table 3 we summarize the critical points  $P_1$  to  $P_6$ , alongside their associated eigenvalues. Furthermore, the stability conditions are the same as discussed in subsection 4.2.1. In summary, in the invariant set  $T = 0$ , the critical points are:

- Point  $P_1$  exists always. It corresponds to a dark-energy dominated solution, i.e.  $\Omega_{DE} = 1$  with  $T = 0$ . It is a stable point for  $-1 < w_m < 1$ ,  $0 < c < 1$ .
- Points  $P_2$  and  $P_3$  exist always. They are two representations of the matter-dominated solution  $\Omega_{DE} = 0$  with  $T = 0$ . They are past attractors, i.e. unstable points, for  $-\frac{1}{3} < w_m \leq 1$ , while they are saddle for  $-1 < w_m < -\frac{1}{3}$ .
- Points  $P_4^\pm$  exist always. They correspond to the dark-energy dominated solution with  $\Omega_{DE} = 1$  with  $T = 0$ . They are unstable points for  $0 < c < \frac{1}{2}$ ,  $-1 \leq w_m \leq 1$ , or  $c \geq \frac{1}{2}$ ,  $-1 \leq w_m < \frac{2-c}{3c}$ , while they are saddle for  $c > \frac{1}{2}$ ,  $\frac{2-c}{3c} < w_m \leq 1$ .
- Points  $P_5$  and  $P_6$  exist for  $-1 \leq \frac{1}{2}c(3w_m + 1) \leq 1$ . They are unstable for  $0 \leq c \leq 1$ ,  $-1 < w_m < -\frac{1}{3}$  or  $c > 1$ ,  $-\frac{c+2}{3c} < w_m < -\frac{1}{3}$ , while for  $0 \leq c < \frac{1}{2}$ ,  $-\frac{1}{3} < w_m \leq 1$ , or  $c \geq \frac{1}{2}$ ,  $-\frac{1}{3} < w_m < \frac{2-c}{3c}$ , they are saddle.

Moreover, the system admits, at most, twelve additional equilibrium points  $(\theta, T)$ , with  $\theta \in \{\theta_1, \theta_2, \theta_3\}$  satisfying  $\cos^2(\theta) = 1$ , and  $T \in \{T_1, T_2, T_3, T_4\}$  satisfying  $\frac{(T-1)^4}{T^4} - \frac{4\beta^2 c^2}{3} = 0$ , explicitly given by (48). Such points with  $0 < T_c < 1$ , corresponding to de Sitter solution  $a(t) \propto e^{H_0 t (\frac{1}{T_c} - 1)}$ , are stable for  $c \geq 1$  or saddle otherwise.

Notice that the physical values are the real values of  $T_i$  satisfying  $0 \leq T_i \leq 1$ ,  $i = 1, 2, 3, 4$ . One eigenvalue is always  $-\frac{3}{2}(1+w_m)$ , while the other one is infinite. The stability conditions are found numerically and, moreover, for  $\beta = 0$  we find  $T_i = 0$ . Hence, we re-obtain points  $P_7$  and  $P_{10}^\pm$  in Table 2. Indeed, for  $\beta = 0$  all the results of section 4.2.1 are recovered.

The solutions of physical interest are those with  $T = 0$ . Point  $P_1$ , which corresponds to a dark-energy dominated solution  $\Omega_{DE} = 1$  with  $T = 0$ , is stable for  $-1 < w_m < 1$ ,  $0 < c < 1$ . Points  $P_2$  and  $P_3$ , which are two representations of the matter-dominated solution  $\Omega_{DE} = 0$  with  $T = 0$ , are past attractors for  $-\frac{1}{3} < w_m \leq 1$  or saddle for  $-1 < w_m < -\frac{1}{3}$ . Points  $P_4^\pm$ , which correspond to a dark-energy dominated solution are unstable for  $0 < c < \frac{1}{2}$ ,  $-1 \leq w_m \leq 1$ , or  $c \geq \frac{1}{2}$ ,  $-1 \leq w_m < \frac{2-c}{3c}$ , while they are saddle points for  $c > \frac{1}{2}$ ,  $\frac{2-c}{3c} < w_m \leq 1$ . Finally, points  $P_5$  and  $P_6$

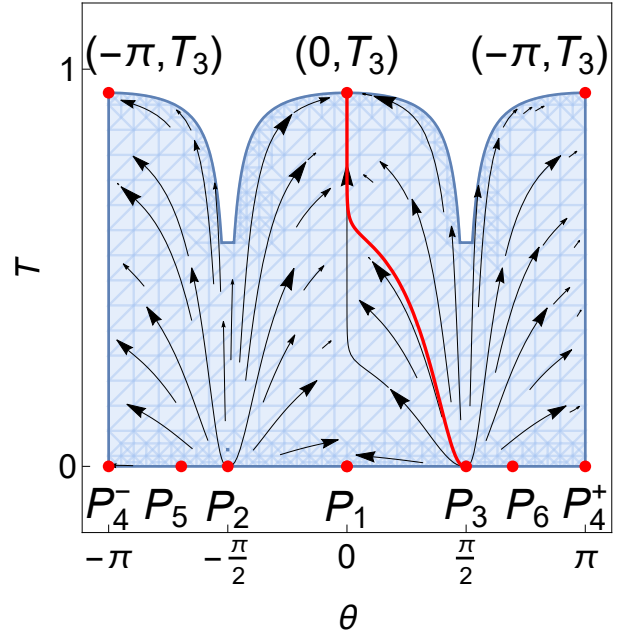


**Figure 7.** Phase-space plot of the dynamical system (53)-(54) for the best fit values  $\beta = -0.003$  and  $c = 1.151$ , and for dust matter ( $w_m = 0$ ). The red curve represents the solution for the initial data  $\Omega_{DE}|_{z=0} = 0.71$  (i.e.,  $\theta(0) = \arccos\left(\frac{1}{10}\sqrt{71}\right) \approx 0.569$ ), corresponding to the mean value from the joint analysis CC+SNIa+BAO, and for  $T|_{z=0} = 0.5$ . The dashed-blue region is the physical region where the equations are real-valued.

exist for  $-1 \leq \frac{1}{2}c(3w_m + 1) \leq 1$ . They are sources for  $0 \leq c \leq 1$ ,  $-1 < w_m < -\frac{1}{3}$  or  $c > 1$ ,  $-\frac{c+2}{3c} < w_m < -\frac{1}{3}$ , while for  $0 \leq c < \frac{1}{2}$ ,  $-\frac{1}{3} < w_m \leq 1$ , or  $c \geq \frac{1}{2}$ ,  $-\frac{1}{3} < w_m < \frac{2-c}{3c}$ , they are saddle. Finally, note that the region where  $T \rightarrow 1$  is contained in the complex-valued domain. This forbids solutions with  $H = 0$ , which appear in the standard-holographic dark energy scenario of (51)-(52).

In Fig. 7 we show a phase-space plot of the system (53)-(54) for the best-fit values  $\beta = -0.003$  and  $c = 1.151$  and for dust matter ( $w_m = 0$ ). In this case the only real value is  $T_3 \approx 0.941$ . At points  $(-\pi, T_3)$ ,  $(0, T_3)$ , and  $(\pi, T_3)$ , the eigenvalues are  $-\frac{3}{2}$  and one eigenvalue is negative infinity at the exact value of  $T_3$ , therefore they are sink. For comparison, we have added the red curve, corresponding to the solution for the initial data  $\Omega_{DE}|_{z=0} = 0.71$  (i.e.,  $\theta(0) = \arccos\left(\frac{1}{10}\sqrt{71}\right) \approx 0.569$ ), which is the mean value from the joint analysis CC+SNIa+BAO, and for  $T|_{z=0} = 0.5$ . From this figure it is confirmed that the late-time attractor is the dark-energy dominated solution (de Sitter solution with  $a(t) \propto e^{H_0 t (\frac{1}{T_c} - 1)}$ ,  $H_0 = h \times 100 \text{ km s}^{-1} \text{ Mpc}^{-1}$ ,  $T_c \approx 0.941$ ,  $h = 0.761$ ), while the past attractor is the matter-dominated solution.

## 5 SUMMARY AND DISCUSSION

We investigated the scenario of Kaniadakis-holographic dark energy scenario by confronting it with observational data. This is an extension of the usual holographic dark-energy model which arises from the use of the generalized Kaniadakis entropy instead of the standard Boltzmann-Gibbs one, which in turn appear from the relativistic extension of standard statistical theory.

We applied the Bayesian approach to extract the likelihood bounds

Label	$(T, \theta)$	Eigenvalues
$P_1$	$(0, 2\pi c_1)$	$\left\{ \frac{c-1}{c}, -\frac{3w_m c + c + 2}{2c} \right\}$
$P_2$	$\left(0, \frac{1}{2}\pi(4c_1 - 1)\right)$	$\left\{ \frac{3(w_m+1)}{2}, \frac{1}{2}(3w_m + 1) \right\}$
$P_3$	$\left(0, \frac{1}{2}\pi(4c_1 + 1)\right)$	$\left\{ \frac{3(w_m+1)}{2}, \frac{1}{2}(3w_m + 1) \right\}$
$P_4^\pm$	$(0, 2\pi c_1 \pm \pi)$	$\left\{ 1 + \frac{1}{c}, -\frac{3w_m}{2} + \frac{1}{c} - \frac{1}{2} \right\}$
$P_5$	$\left(0, \arctan\left[-x, -\sqrt{1-x^2}\right] + 2\pi c_1\right)$	$\left\{ \frac{3(w_m+1)}{2}, \frac{1}{8}(3w_m + 1)(c^2(1+3w_m)^2 - 4) \right\}$
$P_6$	$\left(0, \arctan\left[-x, \sqrt{1-x^2}\right] + 2\pi c_1\right)$	$\left\{ \frac{3(w_m+1)}{2}, \frac{1}{8}(3w_m + 1)(c^2(1+3w_m)^2 - 4) \right\}$

**Table 3.** The critical points and their associated eigenvalues of the system (53)-(54) in the invariant set  $T = 0$ . We use the notation  $x = \frac{1}{2}c(3w_m + 1)$ ,  $c_1 \in \mathbb{Z}$ .

of the Kaniadakis parameter, as well as the other free model parameters. In particular, we performed a Markov Chain Monte Carlo analysis using data from cosmic chronometers, supernovae type Ia, and Baryon Acoustic Oscillations observations. Concerning the Kaniadakis parameter, we found that it is constrained around 0, namely, around the value in which Kaniadakis entropy recovers the standard Bekenstein-Hawking one, as expected. Additionally, for  $\Omega_m^{(0)}$  we obtained a slightly smaller value compared to  $\Lambda$ CDM scenario.

Furthermore, we reconstructed the evolution of the Hubble, deceleration and jerk parameters in the redshift range  $0 < z < 2$ . We find that, within one sigma confidence level with those reported in Herrera-Zamorano et al. (2020), the deceleration-acceleration transition redshift is  $z_T = 0.86^{+0.21}_{-0.14}$ , and the age of the Universe is  $t_U = 13.000^{+0.406}_{-0.350}$  Gyrs. Lastly, we applied the usual information criteria in order to compare the statistical significance of the fittings with  $\Lambda$ CDM cosmology. Both criteria AICc and BIC conclude that the  $\Lambda$ CDM scenario is strongly favored in comparison to Kaniadakis-holographic dark energy.

Finally, we performed a detailed dynamical-system analysis to extract the local and global features of the evolution in the scenario of Kaniadakis-holographic dark energy. We extracted the critical points as well as their stability properties and found that the past attractor of the Universe is the matter-dominated solution, while the late-time stable solution is the dark-energy-dominated one with  $H \rightarrow 0$ .

In summary, Kaniadakis-holographic dark energy presents interesting cosmological behavior and is in agreement with observations. We remark that the scenario may solve the turning point in the Hubble parameter reconstruction of standard holographic dark energy (Colgáin & Sheikh-Jabbari 2021), which violates the NEC, and thus it is an interesting improvement in this context.

## ACKNOWLEDGEMENTS

We thank the anonymous referee for thoughtful remarks and suggestions. Authors acknowledge Eoin O. Colgáin for fruitful comments. G.L. was funded by Agencia Nacional de Investigación y Desarrollo - ANID for financial support through the program FONDECYT Iniciación grant no. 11180126 and by Vicerrectoría de Investigación y Desarrollo Tecnológico at UCN. J.M. acknowledges the support from ANID project Basal AFB-170002 and ANID REDES 190147. M.A.G.-A. acknowledges support from SNI-México, CONACyT research fellow, ANID REDES (190147), Cátedra Marcos Moshinsky and Instituto Avanzado de Cosmología (IAC). A.H.A. thanks to the PRODEP project, Mexico for resources and financial support and thanks also to the support from Luis Aguilar, Alejandro de León, Carlos Flores, and Jair García of the Laboratorio Nacional de Visualización Científica Avanzada. V.M. acknowledges support from Centro de Astrofísica de Valparaíso and ANID REDES 190147. This

work is partially supported by the Ministry of Education and Science of the Republic of Kazakhstan, Grant AP08856912.

## DATA AVAILABILITY

The data underlying this article were cited in Section 3.1.

## REFERENCES

- Abreu E. M. C., Ananias Neto J., 2021, *EPL*, 133, 49001  
 Abreu E. M. C., Ananias Neto J., Barboza E. M., Nunes R. C., 2016, *EPL*, 114, 55001  
 Abreu E. M. C., Neto J. A., Mendes A. C. R., Bonilla A., 2018, *EPL*, 121, 45002  
 Aghanim N., et al., 2018, Planck 2018 results. VI. Cosmological parameters ([arXiv:1807.06209](https://arxiv.org/abs/1807.06209))  
 Aghanim N., et al., 2020, *Astronomy & Astrophysics*, 641, A6  
 Akaïke H., 1974, *IEEE Transactions on Automatic Control*, 19, 716  
 Aylor K., Joy M., Knox L., Millea M., Raghunathan S., Wu W. L. K., 2019, *The Astrophysical Journal*, 874, 4  
 Bhattacharjee S., 2021, *Eur. Phys. J. C*, 81, 217  
 Birrer S., Treu T., 2021, *A&A*, 649, A61  
 Bouhmadi-Lopez M., Errahmani A., Ouali T., 2011, *Phys. Rev. D*, 84, 083508  
 Cai R.-G., 2007, *Phys. Lett. B*, 657, 228  
 Cai Y.-F., Saridakis E. N., Setare M. R., Xia J.-Q., 2010, *Phys. Rept.*, 493, 1  
 Cai Y.-F., Capozziello S., De Laurentis M., Saridakis E. N., 2016, *Rept. Prog. Phys.*, 79, 106901  
 Capozziello S., De Laurentis M., 2011, *Phys. Rept.*, 509, 167  
 Chaplygin S. A., 1904, *Sci. Mem. Moscow Univ. Math. Phys.*, 21  
 Chen X.-m., Gong Y.-g., Saridakis E. N., 2009, *JCAP*, 0904, 001  
 Coley A. A., 2003, *Dynamical systems and cosmology*. Vol. 291, Kluwer, Dordrecht, Netherlands, doi:10.1007/978-94-017-0327-7  
 Colgáin E. O., Sheikh-Jabbari M. M., 2021, *Class. Quant. Grav.*, 38, 177001  
 Copeland E. J., Liddle A. R., Wands D., 1998, *Phys. Rev.*, D57, 4686  
 Copeland E. J., Sami M., Tsujikawa S., 2006, *Int. J. Mod. Phys. D*, 15, 1753  
 Cotsakis S., Kittou G., 2013, *Phys. Rev.*, D88, 083514  
 Cruz M., Cruz N., Lepe S., 2017a, *Phys. Rev. D*, 96, 124020  
 Cruz M., Cruz N., Lepe S., 2017b, *Phys. Rev. D*, 96, 124020  
 Cruz N., Hernández-Almada A., Cornejo-Pérez O., 2019, *Phys. Rev. D*, 100, 083524  
 Dabrowski M. P., Salzano V., 2020, *Phys. Rev. D*, 102, 064047  
 Dainotti M. G., De Simone B., Schiavone T., Montani G., Rinaldi E., Lambiase G., 2021, *The Astrophysical Journal*, 912, 150  
 Di Valentino E., et al., 2021, *Astropart. Phys.*, 131, 102605  
 Drepanou N., Lympers A., Saridakis E. N., Yesmahanova K., 2021, Kaniadakis holographic dark energy ([arXiv:2109.09181](https://arxiv.org/abs/2109.09181))  
 Efstathiou G., 2021, *Mon. Not. Roy. Astron. Soc.*, 505, 3866  
 Feng C., Wang B., Gong Y., Su R.-K., 2007, *JCAP*, 09, 005  
 Ferreira P. G., Joyce M., 1997, *Phys. Rev. Lett.*, 79, 4740  
 Foreman-Mackey D., Hogg D. W., Lang D., Goodman J., 2013, *pasf*, 125, 306

- Freedman W. L., 2021, Measurements of the Hubble Constant: Tensions in Perspective ([arXiv:2106.15656](https://arxiv.org/abs/2106.15656))
- García-Aspeitia M. A., Hernández-Almada A., 2021, *Phys. Dark Univ.*, 32, 100799
- García-Aspeitia M. A., Magaña J., Hernández-Almada A., Motta V., 2017, *Int. J. Mod. Phys. D*, 27, 1850006
- García-Aspeitia M. A., Hernández-Almada A., Magaña J., Amante M. H., Motta V., Martínez-Robles C., 2018, *Phys. Rev. D*, 97, 101301
- García-Aspeitia M. A., Martínez-Robles C., Hernández-Almada A., Magaña J., Motta V., 2019, *Phys. Rev.*, D99, 123525
- García-Aspeitia M. A., Hernández-Almada A., Magaña J., Motta V., 2021, *Phys. Dark Univ.*, 32, 100840
- Giambo R., Miritzis J., 2010, *Class. Quant. Grav.*, 27, 095003
- Glavan D., Lin C., 2020, *Phys. Rev. Lett.*, 124, 081301
- Gong Y.-g., 2004, *Phys. Rev. D*, 70, 064029
- Hernández-Almada, A. Magaña, Juan García-Aspeitia, Miguel A. Motta, V. 2019, *Eur. Phys. J. C*, 79, 12
- Hernández-Almada A., García-Aspeitia M. A., Magaña J., Motta V., 2020a, *Phys. Rev. D*, 101, 063516
- Hernández-Almada A., García-Aspeitia M. A., Magaña J., Motta V., 2020b, *Phys. Rev. D*, 101, 063516
- Hernández-Almada A., Leon G., Magaña J., García-Aspeitia M. A., Motta V., 2020c, *Mon. Not. Roy. Astron. Soc.*, 497, 1590
- Hernández-Almada A., 2019, *Eur. Phys. J. C*, 79, 751
- Herrera-Zamorano L., Hernández-Almada A., García-Aspeitia M. A., 2020, *Eur. Phys. J. C*, 80
- Horvat R., 2004, *Phys. Rev. D*, 70, 087301
- Huang Q., Huang H., Xu B., Tu F., Chen J., 2021, *Eur. Phys. J. C*, 81, 686
- Hurvich C. M., Tsai C. L., 1989, *Biometrika*, 76, 297
- Kaniadakis G., 2002, *Phys. Rev. E*, 66, 056125
- Kaniadakis G., 2005, *Phys. Rev. E*, 72, 036108
- Khurshudyan M., Sadeghi J., Myrzakulov R., Pasqua A., Farahani H., 2014, *Adv. High Energy Phys.*, 2014, 878092
- Kim H., Lee H. W., Myung Y. S., 2006, *Phys. Lett. B*, 632, 605
- Kritpetch C., Muhammad C., Gumjudpai B., 2020, *Phys. Dark Univ.*, 30, 100712
- Leon G., Magaña J., Hernández-Almada A., García-Aspeitia M. A., Verdugo T., Motta V., 2021, Barrow Entropy Cosmology: an observational approach with a hint of stability analysis ([arXiv:2108.10998](https://arxiv.org/abs/2108.10998))
- Li M., 2004, *Phys. Lett. B*, 603, 1
- Li X., Shafieloo A., 2019, *ApJ*, 883, L3
- Li X., Shafieloo A., 2020, arXiv e-prints, [p. arXiv:2001.05103](https://arxiv.org/abs/2001.05103)
- Li M., Li X.-D., Wang S., Zhang X., 2009, *JCAP*, 06, 036
- Lin C., 2021, *Journal of Cosmology and Astroparticle Physics*, 2021, 003
- Lu J., Saridakis E. N., Setare M. R., Xu L., 2010, *JCAP*, 03, 031
- Lymperis A., Basilakos S., Saridakis E. N., 2021, Modified cosmology through Kaniadakis horizon entropy ([arXiv:2108.12366](https://arxiv.org/abs/2108.12366))
- Maartens R., Koyama K., 2010, *Living Rev. Rel.*, 13, 5
- Magaña J., Amante M. H., García-Aspeitia M. A., Motta V., 2018, *Monthly Notices of the Royal Astronomical Society*, 476, 1036
- Mamon A. A., Paliathanasis A., Saha S., 2021, *Eur. Phys. J. Plus*, 136, 134
- Micheletti S. M. R., 2010, *JCAP*, 05, 009
- Moradpour H., Ziaie A. H., Kord Zangeneh M., 2020, *Eur. Phys. J. C*, 80, 732
- Moresco M., et al., 2016, *JCAP*, 1605, 014
- Motta V., García-Aspeitia M. A., Hernández-Almada A., Magaña J., Verdugo T., 2021, *Universe*, 7
- Nadathur S., Percival W. J., Beutler F., Winther H., 2020, *Phys. Rev. Lett.*, 124, 221301
- Nojiri S., Odintsov S. D., 2006, *Gen. Rel. Grav.*, 38, 1285
- Nojiri S., Odintsov S. D., 2017, *Eur. Phys. J. C*, 77, 528
- Nojiri S., Odintsov S. D., Paul T., 2021, *Symmetry*, 13, 928
- Nunes R. C., Yadav S. K., Jesus J. F., Bernui A., 2020, *Monthly Notices of the Royal Astronomical Society*, 497, 2133–2141
- Pan S., Yang W., Di Valentino E., Shafieloo A., Chakraborty S., 2019, arXiv e-prints, [p. arXiv:1907.12551](https://arxiv.org/abs/1907.12551)
- Pavon D., Zimdahl W., 2005, *Phys. Lett. B*, 628, 206
- Perko L., 2000, *Differential Equations and Dynamical Systems*, Third Edition. Springer
- Perlmutter S., Aldering G., Goldhaber G., Knop R. A., Nugent P., others Project T. S. C., 1999, *The Astrophysical Journal*, 517, 565
- Riess A. G., Filippenko A. V., Challis P., Clocchiatti A., Diercks A., et al., 1998, *The Astronomical Journal*, 116, 1009
- Riess A. G., Casertano S., Yuan W., Macri L. M., Scolnic D., 2019, *The Astrophysical Journal*, 876, 85
- Riess A. G., Casertano S., Yuan W., Bowers J. B., Macri L., Zinn J. C., Scolnic D., 2021, *Astrophys. J. Lett.*, 908, L6
- Saridakis E. N., 2008a, *JCAP*, 04, 020
- Saridakis E. N., 2008b, *Phys. Lett. B*, 660, 138
- Saridakis E. N., 2018, *Phys. Rev. D*, 97, 064035
- Saridakis E. N., 2020, *Phys. Rev. D*, 102, 123525
- Saridakis E. N., Basilakos S., 2021, *Eur. Phys. J. C*, 81, 7
- Saridakis E. N., Bamba K., Myrzakulov R., Anagnostopoulos F. K., 2018, *JCAP*, 12, 012
- Saridakis E. N., et al., 2021, Modified Gravity and Cosmology: An Update by the CANTATA Network ([arXiv:2105.12582](https://arxiv.org/abs/2105.12582))
- Schwarz G., 1978, *Ann. Statist.*, 6, 461
- Scolnic D. M., et al., 2018, *Astrophys. J.*, 859, 101
- Setare M. R., Saridakis E. N., 2008, *Phys. Lett. B*, 670, 1
- Setare M. R., Saridakis E. N., 2009, *Phys. Lett. B*, 671, 331
- Setare M. R., Vagenas E. C., 2008, *Phys. Lett. B*, 666, 111
- Shah P., Lemos P., Lahav O., 2021, A buyer's guide to the Hubble Constant ([arXiv:2109.01161](https://arxiv.org/abs/2109.01161))
- Shajib A. J., et al., 2020, *Mon. Not. Roy. Astron. Soc.*, 494, 6072
- Shekh S. H., 2021, *Phys. Dark Univ.*, 33, 100850
- Spergel D. N., et al., 2003, *Astrophys. J. Suppl.*, 148, 175
- Sugiura N., 1978, *Communications in Statistics - Theory and Methods*, 7, 13
- Susskind L., 1995, *Journal of Mathematical Physics*, 36, 6377
- Suwa M., Nihei T., 2010, *Phys. Rev. D*, 81, 023519
- Villanueva J., 2015, *Journal of Cosmology and Astroparticle Physics*, 2015, 045
- Wainwright J., Ellis G. F. R., 1997, *Dynamical Systems in Cosmology*. Cambridge University Press
- Wang B., Gong Y.-g., Abdalla E., 2005, *Phys. Lett. B*, 624, 141
- Wang S., Wang Y., Li M., 2017, *Phys. Rept.*, 696, 1
- Weinberg S., 1989, *Rev. Mod. Phys.*, 61, 1
- Zel'dovich Y., Krasinski A., Zeldovich Y., 1968, *Sov. Phys. Usp.*, 11, 381
- Zhang X., 2009, *Phys. Rev. D*, 79, 103509
- Zhang X., Wu F.-Q., 2005, *Phys. Rev. D*, 72, 043524
- da Silva W. J. C., Silva R., 2021, *Eur. Phys. J. Plus*, 136, 543
- 't Hooft G., 1993, arXiv e-prints, [pp gr-qc/9310026](https://arxiv.org/abs/gr-qc/9310026)

This paper has been typeset from a  $\text{\TeX}/\text{\LaTeX}$  file prepared by the author.